Available online at www.sciencedirect.com
ScienceDirect
Biochemical and Biophysical Research Communications 367 (2008) 590–596
BBRC
www.elsevier.com/locate/ybbrc

Prostaglandin $F_{2\alpha}$ regulates cytokine responses of mast cells through the receptors for prostaglandin E

Izumi Kaneko [a], Takanori Hishinuma [b], Kaori Suzuki [b], Yuji Owada [c], Noriko Kitanaka [c], Hisatake Kondo [c], Junichi Goto [d], Hiroshi Furukawa [a], Masao Ono [a,*]

[a] *Department of Pathology, Tohoku University Graduate School of Medicine, 2-1 Seiryo, Aoba-ku, Sendai, Miyagi 980-8575, Japan*
[b] *Division of Pharmacotherapy, Graduate School of Pharmaceutical Sciences, Tohoku University, Sendai, Japan*
[c] *Department of Histology, Tohoku University Graduate School of Medicine, Sendai, Japan*
[d] *Division of Clinical Pharmacology, Tohoku University Hospital, Sendai, Japan*

Received 28 December 2007
Available online 9 January 2008

Abstract

There is an increasing body of evidence that prostanoids modulate mast cell functions and contribute to the development of allergic inflammation. The present study aimed to identify an undetermined function of prostaglandin (PG) $F_{2\alpha}$ in mast cell activation and the signaling mechanism involved in it. Simultaneous quantification of prostanoids by liquid chromatography/tandem mass spectrometry revealed the constitutive release of $PGF_{2\alpha}$, thromboxane B_2, and 6-keto-$PGF_{1\alpha}$ from bone marrow-derived mast cells (BMMCs). Upon activation of BMMCs by lipopolysaccharide, the cytokine production in BMMCs was enhanced when the culture was supplemented with $PGF_{2\alpha}$. However, F prostanoid receptor—a selective receptor for $PGF_{2\alpha}$—was not detected in BMMCs. Further investigations performed using prostanoid receptor antagonists revealed an alternative mechanism wherein the receptors for PGE species—E prostanoid receptors—mediated the $PGF_{2\alpha}$ signal in BMMCs. The present study provides an insight into a novel function of $PGF_{2\alpha}$, i.e., an autocrine accelerator for mast cell activation.

Keywords: Mast cell; Lipid mediator; $PGF_{2\alpha}$; Lipopolysaccharide; E prostanoid receptor; EP; Autocrine

Mast cells play a role in the immune and inflammatory responses by sensing a variety of pathogenic patterns through cell-surface receptors. The recruitment of a high-affinity Fc receptor for IgE (FcεRI) by IgE and antigen (hereafter denoted as IgE/Ag) initiates the release of a variety of inflammatory mediators, including histamines, lipid metabolites, and cytokines, occasionally entailing the onset of immediate hypersensitivity and allergic inflammation. On the other hand, mast cells also recognize pathogens in an innate immune mode through other receptors, thus contributing to host defense against bacterial and viral infections. This recognition is mainly achieved by a member of the toll-like receptor (TLR) family, and it subsequently triggers the release of proinflammatory cytokines, including interferons, interleukins, and tumor necrosis factor (TNF)-α, which act in the elimination of pathogens by activating and mobilizing inflammatory cells toward infected sites. Recent studies have shown that a bacterial component, namely, lipopolysaccharide (LPS), enhances FcεRI-mediated mast cell activation [1,2]. Indeed, the co-occurrence of infectious events and the exacerbation of allergic manifestation has been demonstrated in allergic human populations [3–5]. Current findings implicate the contribution of TLR-mediated mast cell activation to the hypersensitivity in allergic diseases in humans.

Membrane lipid metabolites such as prostaglandins (PGs) and leukotrienes (LTs) have been characterized as early mediators that influence the onset of allergic inflammation in mouse models [6–8]. A recent study showed that when the culture of bone marrow-derived mast cells

* Corresponding author. Fax: +81 22 717 8503.
E-mail address: onomasao@mail.tains.tohoku.ac.jp (M. Ono).

0006-291X/$ - see front matter © 2008 Elsevier Inc. All rights reserved.
doi:10.1016/j.bbrc.2008.01.002

(BMMCs) was supplemented with PGE_2 interleukin (IL)-6 production was remarkably enhanced following IgE/Ag simulation [9]. Another study using antagonists specific to an E prostanoid receptor (EP) has shown that EP3 mediates a signal that enhances mast cell activation when supplemented with PGE_2, while EP2 mediates a suppressive signal under the same condition [10]. A study performed using BMMCs derived from EP-deficient strains of mice has proven that EP3 is essential for IL-6 production and degranulation of BMMCs [11]. These findings indicate the contribution of EP2 and EP3 in the regulation of mast cell activation. However, there is little evidence for their role in the production of PGE_1 or PGE_2 in mast cell activation. Paracrine PGE species are considered to be involved in the EP-mediated effects on *in vivo* mast cell activation.

In the present study, we investigated the mechanism of prostanoid-mediated mast cell activation following LPS stimulation using BMMCs. Highly sensitive and simultaneous quantification of prostanoids performed using liquid chromatography/tandem mass spectrometry (LC/MS-MS) revealed constitutive release of $PGF_{2\alpha}$, thromboxane (TX) B_2, and 6-keto-$PGF_{1\alpha}$ into the cultured medium. Functional analyses performed using $PGF_{2\alpha}$ and EP antagonists revealed an enhancing effect of $PGF_{2\alpha}$ on mast cell activation through its heterologous binding to EPs. The present findings provide a novel insight into the role of $PGF_{2\alpha}$ in the regulation of allergenic mast cell response.

Materials and methods

Preparation and activation of BMMC. BMMCs were obtained by culturing mouse bone marrow cells in the RPMI 1640 supplemented with 10% FCS, 1 mM sodium pyruvate, non-essential amino acids, 50 μM 2-mercaptoethanol (SIGMA, St. Louis, MO), and 5 ng/ml murine IL-3 (R&D Systems, Minneapolis, MN). BMMCs were activated with 1 μg/ml trinitrophenyl (TNP) hapten-specific IgE (TNP-IgE) and 1 ng/ml of TNP-conjugated ovalbumin (TNP-OVA) (fraction VII, SIGMA). LPS (*Escherichia coli* 055:B5, SIGMA) was used for the stimulation at 0.1 μg/ml. A cyclooxygenase (Cox) inhibitor, 5-lipooxygenase (Lox) inhibitor, or EP antagonist was incubated for 30 min prior to the supplementation of PG. $PGF_{2\alpha}$, PGE_2, PGD_2 (Cayman chemical, Ann Arbor, MI), and FP agonist Fluprostenol (BIOMOL, Plymouth Meeting, PA) were dissolved in ethanol and were added to the BMMC culture, then incubated for 20 min prior to the stimulation. EP antagonists—ONO-8711 (EP1 antagonist), ONO-AE3-240 (EP3 antagonist), and ONO-AE3-208 (EP4 antagonist)—were kindly donated from Ono pharmaceutics Co. Ltd., Osaka, Japan. Indomethacin (WAKO Pure Chemical, Osaka, Japan), NS-398, SC-560, and NDGA (Cayman chemical) were dissolved in DMSO or ethanol and were added to the BMMC culture with a constant solvent concentration (0.1% DMSO or ethanol). All experiments were performed under non-toxic conditions for any inhibitor dose, which were assessed by cell viability test (data not shown).

Measurements of cytokines and degranulation of BMMC. The concentration of IL-6 and TNF-α in the cultured medium were measured at 6 h after stimulation by enzyme-linked immunosorbent assay (ELISA) kits (BD PharMingen, San Diego, CA).

Liquid chromatography/tandem mass spectrometry (LC/MS-MS) analysis. Simultaneous quantification of PGs and TXB_2 were performed as previously described [12]. Briefly, the cultured medium collected at 1 h after the stimulations were subjected to analysis by LC/MS-MS. $PGF_{2\alpha\text{-}d4}$, $PGE_{2\text{-}d4}$, $PGD_{2\text{-}d4}$, 6-keto-$PGF_{1\alpha\text{-}d4}$, and $TXB_{2\text{-}d4}$ (each 2 ng) were added into the cultured medium (0.2 ml) as an internal standard. The sample was acidified and passed through an Empore C18 HD disk cartridge (3 M Industry, St. Paul, MN). The bound fraction was collected in hexane-ethylacetate (1:2, v/v, 1 ml) as a PG-enriched fraction. After evaporating solvent, the residue was reconstituted in mobile phase (30 μl), sonicated for 30 s, and filtered. The reconstituted sample was transferred to an autosampler vial; 10 μl was subjected to the LC/MS-MS analysis. For the HPLC part, chromatography was performed on a C18 Capcell Pak MGII (1.5 × 150 mm, 5 μm) (Shiseido, Tokyo, Japan) using isocratic elution with acetonitrile–water–acetic acid (40:60:0.02 v/v) at a flow rate of 100 μl/min at 40 °C. The selected reaction monitoring was performed as previously described conditions [12].

Reverse transcriptase-polymerase chain reaction (RT-PCR). Total RNA was purified from kidney, brain, and BMMCs by using a TRIzol™ reagent (Invitrogen, Carlsbad, CA). The complementary DNA (cDNA) was prepared from 1 μg of total RNA with random hexamers and reverse transcriptase SuperScript III™ (Invitrogen). Polymerase chain reaction (PCR) was performed with following primers: 5′-GCTCTTGGTGT TTCCTTCTCG-3′ and 5′-TGCTTGCTGGCTCTCCTTCTC-3′ for a mouse F prostanoid receptor (FP) (446 bp), and 5′-CAGGAGATGG CCACTGCCGCA-3′ and 5′-CTCCTTCTGCATCCTGTCAGCA-3′ for mouse β-actin (276 bp). The annealing temperature in the PCR was set at 60 °C for FP and 52 °C for β-actin.

Statistical analysis. Difference between two mean values was evaluated by two-tail *t*-test or, in case of multiple comparison, the *t*-test combined with Bonferroni correction following ANOVA. P value less than 0.05 was regarded as statistically significant.

Results and discussion

Autocrine PGs influence cytokine production on TLR4-mediated BMMC activation

To estimate the role of autocrine PGs and LTs in LPS-dependent BMMC activation, the inhibitory effect of the Cox or 5-Lox inhibitor was measured by examining the effect on cytokine production. The Cox and Lox inhibitors significantly suppressed IL-6 production (Fig. 1A). The Cox-selective inhibitors NS398 and SC560 did not significantly inhibit TNF-α production; however, the other inhibitors significantly suppressed TNF-α production (Fig. 1B). These findings indicate the role of autocrine PGs and LTs in enhancing cytokine production following TLR4-mediated BMMC activation.

BMMCs constitutively produce $PGF_{2\alpha}$, TXB_2, and 6-keto-$PGF_{1\alpha}$

To identify the autocrine PGs from BMMCs, we simultaneously measured the cumulative amounts of $PGF_{2\alpha}$, PGE_2, PGD_2, 6-keto-$PGF_{1\alpha}$ as PGI_2 metabolites and PGJ_2 and TXB_2 as TXA2 metabolites in the BMMC culture medium by LC/MS-MS, as described previously [12]. The following three culture conditions were tested: untreated, treated with LPS (100 ng/ml), and treated with IgE/Ag (1 ng/ml TNP-OVA). A significant amount of $PGF_{2\alpha}$, TXB_2, and 6-keto-$PGF_{1\alpha}$ was detected under all the conditions (Table 1). $PGF_{2\alpha}$ and 6-keto-$PGF_{1\alpha}$ were undetectable in the culture medium, and an increase of TXB_2 was detected in the presence of BMMC, indicating that $PGF_{2\alpha}$, TXB_2, and 6-keto-$PGF_{1\alpha}$ are constitutively released from BMMCs. The stimulation with IgE/Ag but

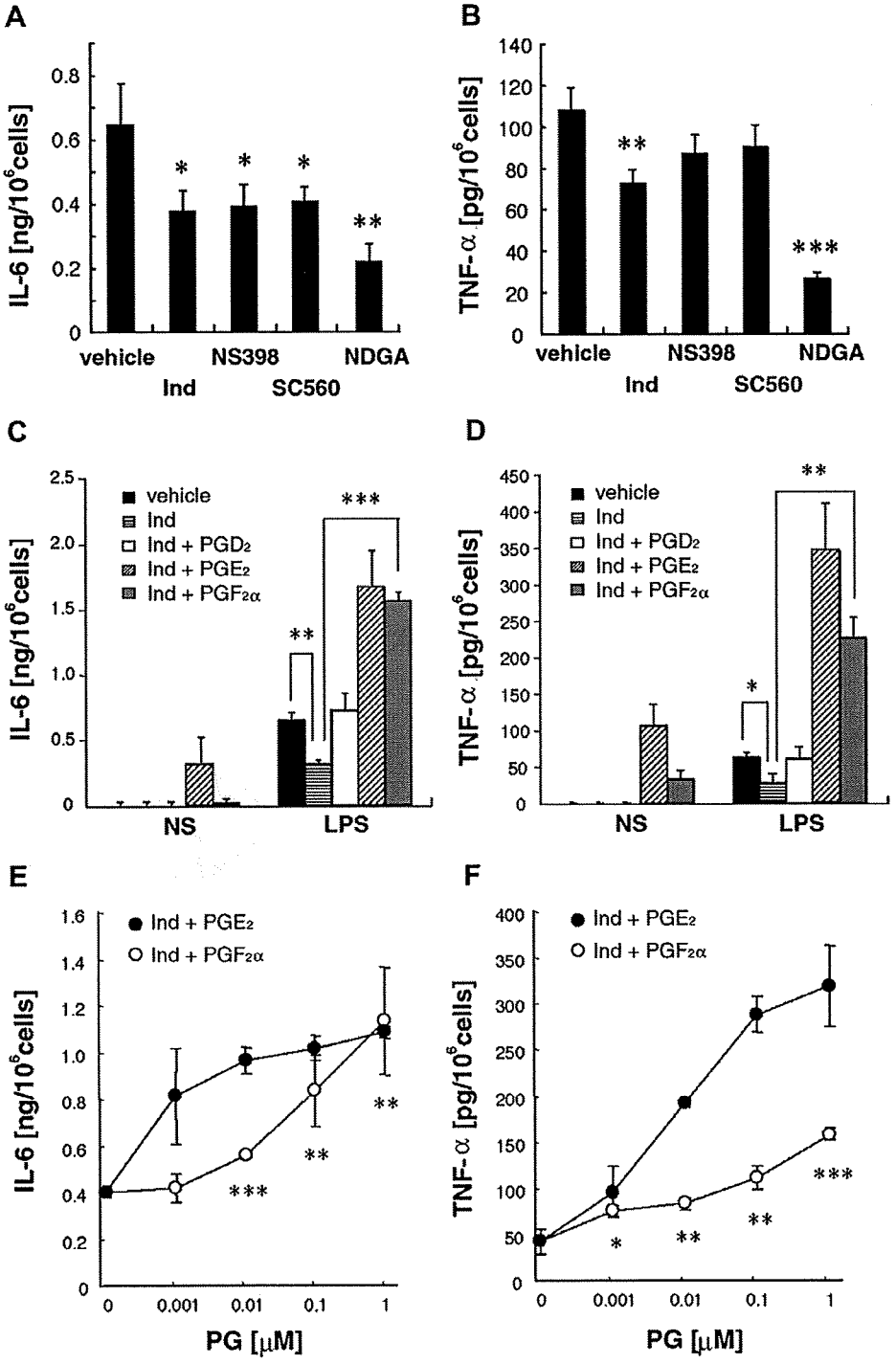

Fig. 1. Effect of deprivation and supplementation of PGs on LPS-induced cytokine responses of BMMCs. (A and B) Effect of Cox or Lox inhibition on LPS-induced cytokine response. BMMCs were cultured for 30 min with 10 μM indomethacin (Ind), 10 μM NS-398 (NS398), 20 nM SC560 (SC560), 10 μM NDGA (NDGA), or ethanol (vehicle), and then stimulated for 6 h with LPS (0.1 μg/ml). (C and D) Effect of supplemented PG on untreated or LPS-induced cytokine response. BMMCs were incubated for 30 min with 10 μM indomethacin (Ind) or DMSO (vehicle), further incubated for 20 min with 1 μM of PGD_2, PGE_2, $PGF_{2\alpha}$, or ethanol, then stimulated for 6 h with LPS (0.1 μg/ml). (E and F) The relationship between a PG dose and cytokine response of BMMCs. BMMCs were treated with PGs (0.001–1 μM). A bar represents SD of triplicate samples. Significant differences are shown: $^{*}p < 0.05$; $^{**}p < 0.01$; $^{***}p < 0.001$. The significant differences were confirmed by two experiments.

not LPS increased the release of $PGF_{2\alpha}$ and TXB_2 by 340% and 200%, respectively, of the resting level. Prior to the present study, Schleimer et al. first measured $PGF_{2\alpha}$ in the culture medium of human lung mast cells by radioimmunoassay and estimated the concentration under the untreated and IgE/Ag-induced conditions as 0.3 ng/10^6

Table 1
Quantification of BMMC-derived prostanoids and thromboxane in cultured medium[a]

	PGD_2 (pg/10^6 cells)	PGE_2 (pg/10^6 cells)	$PGF_{2\alpha}$ (pg/10^6 cells)	PGJ_2 (pg/10^6 cells)	TXB_2 (pg/10^6 cells)	6-Keto $PGF_{1\alpha}$ (pg/10^6 cells)
Medium	<10	<10	<10	<10	166 (45.5)	<10
Untreated	<10	<10	84.2 (50.2)	<10	791 (128)	253 (25.6)
LPS	<10	<10	60.0 (15.9)	<10	701 (121)	98.6 (35.6)
IgE/Ag	890 (236)	<10	288 (47.9)	<10	1593 (320)	88.6 (26.0)

[a] Values denote a mean (SD) of eicosanoid concentration of six independent samples prepared from an experiment. BMMCs were stimulated without (untreated) or with 0.1 μg/ml LPS (LPS), or 1 ng/ml TNP-OVA following IgE sensitization (IgE/Ag). Culture supernatants were collected at 1 h after stimulation. PG, prostaglandin; TX, thromboxane.

cells and 3.3 ng/10^6 cells, respectively [13]. These amounts of $PGF_{2\alpha}$ are mostly comparable to our results. PGD_2 was detected on IgE/Ag stimulation, as previously reported [14–16]. PGE_2 and PGJ_2 were undetectable under all the conditions.

$PGF_{2\alpha}$ enhances TLR4-mediated mast cell responses

Each effect of supplementation with $PGF_{2\alpha}$ and PGE_2 on the cytokine response of BMMCs was evaluated under a condition in which the production of endogenous PGs was prevented by blocking their *de novo* syntheses with indomethacin. $PGF_{2\alpha}$ as well as PGE_2 remarkably enhanced LPS-induced IL-6 (Fig. 1C) and TNF-α production (Fig. 1D). In the absence of stimulation, PGE_2-induced the production of both IL-6 and TNF-α; however, $PGF_{2\alpha}$-induced TNF-α to a lesser extent than PGE_2. PGD_2 had little effect on the cytokine production of BMMCs. The enhancement of the LPS-dependent responses by $PGF_{2\alpha}$ was observed in a dose-dependent manner (Fig. 1E and F). However, the dose–effect relationship demonstrated that $PGF_{2\alpha}$ was less effective in enhancing the LPS-dependent responses than PGE_2.

With regard to the observed effect of $PGF_{2\alpha}$, three possible mechanisms remained to be clarified at this time: the direct effect of $PGF_{2\alpha}$, the effect of conversion of the $PGF_{2\alpha}$ to PGE_2, and the effect of the contamination of PGE_2. The conversion of $PGF_{2\alpha}$ to PGE2 occurs by the action of 9-keto reductase. This enzymatic activity in untreated and stimulated BMMCs was roughly estimated by measuring the *de novo* PGE_2 synthesis in the culture incubated with $PGF_{2\alpha}$ and an excess of the BMMC lysate. There was no detectable PGE2 after the incubation (data not shown). We also estimated the level of contamination of the $PGF_{2\alpha}$ used in this study with PGE_2. The results showed that the contamination level was no higher than 0.01% of the amount of $PGF_{2\alpha}$ input (data not shown). If PGE_2 contamination was maximum in the $PGF_{2\alpha}$-supplemented culture, its effect could not have reached the level achieved by the same amount of purified PGE_2 (Fig. 1E and F). The overall findings suggest that the direct effect of $PGF_{2\alpha}$ is responsible for the enhancement of TLR-mediated mast cell responses.

There is a growing interest in understanding novel $PGF_{2\alpha}$ functions. $PGF_{2\alpha}$ has been shown to exert pleiotropic effects in a variety of pathophysiological conditions through a selective prostanoid receptor for $PGF_{2\alpha}$ (FP). The activation of FP results in an increase in the cytosolic ionic calcium and cyclic AMP concentrations and leads to the contraction of muscle fibers in smooth muscle cells [17,18]. Therefore, FP agonists, such as fluprostenol, have been used in the treatment of patients with glaucoma and for inducing labor. Recently, topical application of an FP agonist on mouse dorsal skin has been shown to stimulate hair growth [19]. FP has been shown to be expressed in the

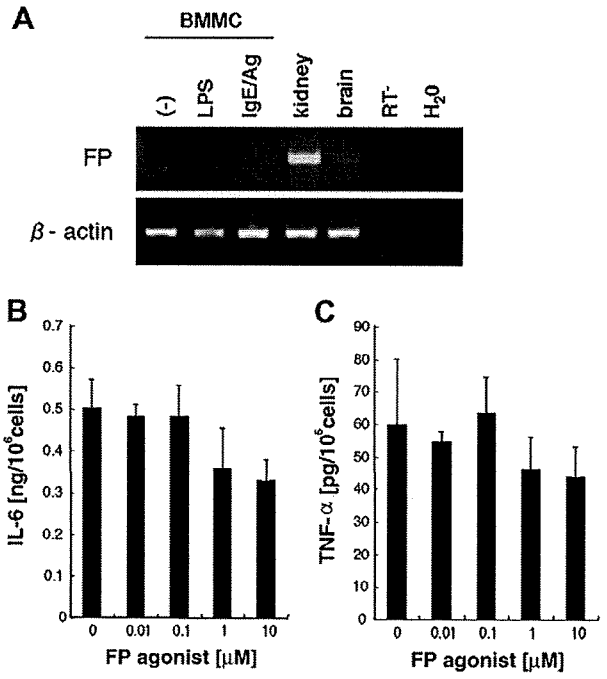

Fig. 2. Expression and function of an F prostanoid receptor (FP) in BMMCs. (A) Undetectable expression of FP in BMMCs revealed by RT-PCR with FP specific primers. Total RNA was isolated from BMMC untreated (−), LPS-induced (LPS), and IgE/Ag-induced (IgE/Ag) BMMCs, and kidney (kidney), and whole brain (brain). BMMCs were treated for 2 h with LPS (0.1 μg/ml) or TNP-specific IgE (1 μg/ml) and TNP-OVA (1 ng/ml). PCR products were visualized by ethidium bromide staining on 2% agarose gel. Amplification of β-actin shows the presence of complementary DNA in RT-PCR. A sample without RT reaction (RT^-) and water (H_2O) were used as negative references. (B and C) Unresponsiveness of BMMCs to an FP-selective agonist—fluporstenol. BMMCs were treated with LPS in the presence of indomethacin and, in place of a PG, 1 μM fluprostenol as performed in this figure. A bar represents SD of triplicate samples. Similar findings that was without statistical significance were obtained from two independent experiments.

collecting duct of the kidneys and regulate water absorption [20]. On the other hand, the presence of TXB_2 and 6-keto-$PGF_{1\alpha}$ in the cultured medium of BMMCs indicates spontaneous production of TXA_2 and PGI_2 from BMMCs. Previous studies have provided evidences for the production of TXB_2 and 6-keto-$PGF_{1\alpha}$ in human lung mast cells and rat serosal mast cells, respectively [13,21]. Other studies have shown that BMMCs respond to PGI_2 [11], and that mastocytoma P815 cells express a selective prostanoid receptor to PGI_2 [22]. The expression of the TXA_2 receptor has not been shown in mast cells [23]. Our present findings provide a novel insight that autocrine PGs regulate mast cell functions and, as a pathologic consequence, influence allergic manifestations in humans.

A selective prostanoid receptor for $PGF_{2\alpha}$ is neither expressed nor functioning in BMMCs

Our findings suggested the presence of a functional receptor for $PGF_{2\alpha}$ in BMMCs. Since the expression of FP in BMMCs had not been observed yet, we examined the expression of FP by reverse transcriptase-polymerase chain reaction (RT-PCR) by using an FP-selective agonist, namely, fluprostenol. The RT-PCR failed to show the expression of FP in untreated and stimulated BMMCs (Fig. 2A). Further, fluprostenol was shown to have no effect on the TLR4-mediated cytokine response of BMMCs (Fig. 2B). These findings suggest the absence of FP in BMMCs and favor a possibility that prostanoid receptor(s)

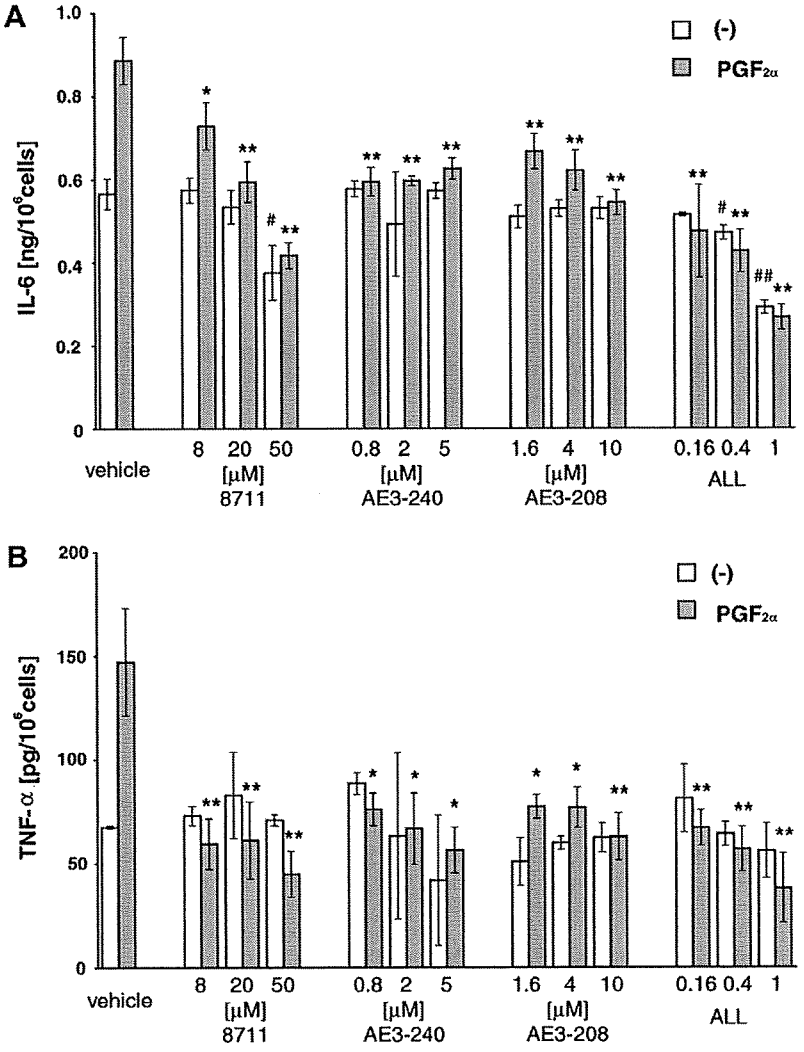

Fig. 3. Blocking effect of EP antagonist(s) on LPS-induced cytokine responses. BMMCs were incubated for 30 min with EP1 antagonist (ONO-8711, 8711), EP3 antagonist (ONO-AE3-240, AE3-240), EP4 antagonist (ONO-AE3-208, AE3-208), a mixture of three EP antagonists (ALL), or DMSO (vehicle), and then incubated for another 20 min with ethanol (white column) or 1 μM $PGF_{2\alpha}$ (gray column). The pretreated BMMCs were stimulated for 6 h with 0.1 μg/ml LPS. DMSO concentration was uniformed at 0.1% for the single antagonist use or 0.25% for the mixture use of three antagonists. For the mixture use, a mixture of 50 μM ONO-8711, 5 μM ONO-AE3-240, and 10 μM ONO-AE3-208 was arbitrarily defined as 1 U in this study. A bar represents SD of triplicate samples. Significant differences are shown: $^{*}p < 0.05$; $^{**}p < 0.01$ (vs vehicle with $PGF_{2\alpha}$); $^{\#}p < 0.05$; $^{\#\#}p < 0.01$ (vs vehicle with (−)).The significant differences were confirmed by other two experiments.

other than FP is (are) present in BMMCs to mediate the $PGF_{2\alpha}$-dependent effect.

Prostanoid receptors for PGE_2 mediate $PGF_{2\alpha}$ signals in BMMCs

Previous studies have shown that $PGF_{2\alpha}$ binds to EP1 and EP3 *in vitro*, although this heterologous association occurs with an affinity that is lower than that between PGE_2 and these receptors [24,25]. Since BMMCs have been shown to express all the four EPs, i.e., EP1, EP2, EP3, and EP4 [11], it is possible that EPs mediated the $PGF_{2\alpha}$ signals in the present experimental conditions. To test this possibility, we performed experiments using EP-selective antagonists—ONO-8711, ONO-AE3-240, and ONO-AE3-208—which have been shown to inhibit the signal of EP1, EP3, and EP4, respectively [26,27]. Two conditions with or without $PGF_{2\alpha}$ were adopted in these experiments. As a result, the augmented fraction, which is shown as the difference between the neighboring white and gray columns in Fig. 3, was significantly decreased by each of the EP antagonists as well as a mixture of all three of them. The decrease in the IL-6 response by EP1 and EP4 and in the TNF-α response by EP4 was observed in a dose-dependent manner. These findings indicate that EP1, EP3, and EP4 are potent receptors for mediating $PGF_{2\alpha}$ signals in BMMCs. Moreover, it should be noted that in the culture condition without $PGF_{2\alpha}$ supplementation, either the EP1 antagonist or the mixture containing all three antagonists significantly inhibited the IL-6 response. This finding implicates the role of endogenous $PGF_{2\alpha}$ in the cytokine response of BMMCs though EPs.

This is the first study that has identified the allergenic *in vitro* effect of $PGF_{2\alpha}$ on mast cell activation and the functional interaction between $PGF_{2\alpha}$ and EPs in mast cells. In other studies, a higher level of $PGF_{2\alpha}$ was detected in the bronchoalveolar lavages of asthmatic patients, although the cells producing $PGF_{2\alpha}$ were unidentified in these cases [28,29]. These findings encourage further investigation of whether the mechanism proposed by us is implicated in the pathogenesis of allergic diseases in humans.

References

[1] H. Qiao, M.V. Andrade, F.A. Lisboa, K. Morgan, M.A. Beaven, FcεR1 and toll-like receptors mediate synergistic signals to markedly augment production of inflammatory cytokines in murine mast cells, Blood 107 (2006) 610–618.

[2] Y.I. Nigo, M. Yamashita, K. Hirahara, R. Shinnakasu, M. Inami, M. Kimura, A. Hasegawa, Y. Kohno, T. Nakayama, Regulation of allergic airway inflammation through toll-like receptor 4-mediated modification of mast cell function, Proc. Natl. Acad. Sci. USA 103 (2006) 2286–2291.

[3] C. Braun-Fahrlander, J. Riedler, U. Herz, W. Eder, M. Waser, L. Grize, S. Maisch, D. Carr, F. Gerlach, A. Bufe, R.P. Lauener, R. Schierl, H. Renz, D. Nowak, E. von Mutius, The Allergy and Endotoxin Study Team, Environmental exposure to endotoxin and its relation to asthma in school-age children, N. Engl. J. Med. 34 (2002) 869–877.

[4] R. Friedman, M. Ackerman, E. Wald, M. Casselbrant, G. Friday, P. Fireman, Asthma and bacterial sinusitis in children, J. Allergy. Clin. Immunol. 74 (1984) 185–189.

[5] B.S. Baker, The role of microorganisms in atopic dermatitis, Clin. Exp. Immunol. 144 (2006) 1–9.

[6] S.G. Trivedi, J. Newson, R. Rajakariar, T.S. Jacques, R. Hannon, Y. Kanaoka, N. Eguchi, P. Colville-Nash, D.W. Gilroy, Essential role for hematopoietic prostaglandin D2 synthase in the control of delayed type hypersensitivity, Proc. Natl. Acad. Sci. USA 103 (2006) 5179–5184.

[7] K. Kabashima, D. Sakata, M. Nagamachi, Y. Miyachi, K. Inaba, S. Narumiya, Prostaglandin E2-EP4 signaling initiates skin immune responses by promoting migration and maturation of Langerhans cells, Nat. Med. 9 (2003) 744–749.

[8] N. Miyahara, K. Takeda, S. Miyahara, C. Taube, A. Joetham, T. Koya, S. Matsubara, A. Dakhama, A.M. Tager, A.D. Luster, E.W. Gelfand, Leukotriene B4 receptor-1 is essential for allergen-mediated recruitment of CD8+ T cells and airway hyperresponsiveness, J. Immunol. 174 (2005) 4979–4984.

[9] I. Leal-Berumen, P. O'Byrne, A. Gupta, C. Richards, J. Marshall, Prostanoid enhancement of interleukin-6 production by rat peritoneal mast cells, J. Immunol. 154 (1995) 4759–4767.

[10] C. Feng, E.M. Beller, S. Bagga, J.A. Boyce, Human mast cells express multiple EP receptors for prostaglandin E2 that differentially modulate activation responses, Blood 107 (2006) 3243–3250.

[11] M. Nguyen, M. Solle, L.P. Audoly, S.L. Tilley, J.L. Stock, J.D. McNeish, T.M. Coffman, D. Dombrowicz, B.H. Koller, Receptors and signaling mechanisms required for prostaglandin E2-mediated regulation of mast cell degranulation and IL-6 production, J. Immunol. 169 (2002) 4586–4593.

[12] T. Hishinuma, K. Suzuki, M. Saito, Y. Hamaguchi, N. Suzuki, Y. Tomioka, I. Kaneko, M. Ono, J. Goto, Simultaneous quantification of seven prostanoids using liquid chromatography/tandem mass spectrometry: the effects of arachidonic acid on prostanoid production in mouse bone marrow-derived mast cells, Prostaglandins Leukot. Essent. Fatty Acids 76 (2007) 321–329.

[13] R.P. Schleimer, E.S. Schulman, D.W. MacGlashan Jr., S.P. Peters, E.C. Hayes, G.K. Adams 3rd., L.M. Lichtenstein, N.F. Adkinson Jr., Effects of dexamethasone on mediator release from human lung fragments and purified human lung mast cells, J. Clin. Invest. 71 (1983) 1830–1835.

[14] F. Levi-Schaffer, E. Dayton, K. Austen, A. Hein, J. Caulfield, P. Gravallese, F. Liu, R. Stevens, Mouse bone marrow-derived mast cells cocultured with fibroblasts. Morphology and stimulation-induced release of histamine, leukotriene B4, leukotriene C4, and prostaglandin D2, J. Immunol. 139 (1987) 3431–3441.

[15] C. Pitton, L. Michel, P. Salem, M. Benhamou, J. Mencia-Huerta, J. Maclouf, C. Prost, C. Burtin, L. Dubertret, J. Benveniste, Biochemical and morphological modifications in dexamethasone-treated mouse bone marrow-derived mast cells, J. Immunol. 141 (1988) 2437–2444.

[16] J. Robin, D. Seldin, K. Austen, R. Lewis, Regulation of mediator release from mouse bone marrow-derived mast cells by glucocorticoids, J. Immunol. 135 (1985) 2719–2726.

[17] W. Chen, T. Andom, P. Bhattacherjee, C. Paterson, Intracellular calcium mobilization following prostaglandin receptor activation in human ciliary muscle cells, Curr. Eye. Res. 16 (1997) 847–853.

[18] B.W. Griffin, P.E. Magnino, I.-H. Pang, N.A. Sharif, Pharmacological characterization of an FP prostaglandin receptor on rat vascular smooth muscle cells (A7r5) Coupled to phosphoinositide turnover and intracellular calcium mobilization, J. Pharmacol. Exp. Ther. 286 (1998) 411–418.

[19] S. Sasaki, Y. Hozumi, S. Kondo, Influence of prostaglandin F2 and its analogues on hair regrowth and follicular melanogenesis in a murine model, Exp. Dermatol. 14 (2005) 323–328.

[20] R.L. Hebert, M. Carmosino, O. Saito, G. Yang, C.A. Jackson, Z. Qi, R.M. Breyer, C. Natarajan, A.N. Hata, Y. Zhang, Y. Guan, M.D. Breyer, Characterization of a rabbit kidney prostaglandin F_{2a}

receptor exhibiting G(i)-restricted signaling that inhibits water absorption in the collecting duct, J. Biol. Chem. 280 (2005) 35028–35037.
[21] R.A. Lewis, N.A. Soter, P.T. Diamond, K.F. Austen, J.A. Oates, L.J. Roberts 2nd., Prostaglandin D2 generation after activation of rat and human mast cells with anti-IgE, J. Immunol. 129 (1982) 1627–1631.
[22] N. Hatae, A. Kita, S. Tanaka, Y. Sugimoto, A. Ichikawa, Induction of adherent activity in mastocytoma P-815 cells by the cooperation of two prostaglandin E2 receptor subtypes, EP3 and EP4, J. Biol. Chem. 278 (2003) 17977–17981.
[23] K.A. Knauer, J.E. Fish, N.F. Adkinson Jr., L.M. Lichtenstein, S.P. Peters, H.H. Newball, Platelet activation in antigen-induced bronchoconstriction, N. Engl. J. Med. 305 (1981) 892–893.
[24] A. Watabe, Y. Sugimoto, A. Honda, A. Irie, T. Namba, M. Negishi, S. Ito, S. Narumiya, A. Ichikawa, Cloning and expression of cDNA for a mouse EP1 subtype of prostaglandin E receptor, J. Biol. Chem. 268 (1993) 20175–20178.
[25] Y. Sugimoto, T. Namba, A. Honda, Y. Hayashi, M. Negishi, A. Ichikawa, S. Narumiya, Cloning and expression of a cDNA for mouse prostaglandin E receptor EP3 subtype, J. Biol. Chem. 267 (1992) 6463–6466.
[26] K. Watanabe, T. Kawamori, S. Nakatsugi, T. Ohta, S. Ohuchida, H. Yamamoto, T. Maruyama, K. Kondo, F. Ushikubi, S. Narumiya, T. Sugimura, K. Wakabayashi, Role of the prostaglandin E receptor subtype EP1 in colon carcinogenesis, Cancer Res. 15 (1999) 5093–5096.
[27] I. Takasaki, H. Nojima, K. Shiraki, Y. Sugimoto, A. Ichikawa, F. Ushikubi, S. Narumiya, Y. Kuraishi, Involvement of cyclooxygenase-2 and EP3 prostaglandin receptor in acute herpetic but not postherpetic pain in mice, Neuropharmacology 49 (2005) 283–292.
[28] M.C. Liu, E.R. Bleecker, L.M. Lichtenstein, A. Kagey-Sobotka, Y. Niv, T.L. McLemore, S. Permutt, D. Proud, W.C. Hubbard, Evidence for elevated levels of histamine, prostaglandin D2, and other bronchoconstricting prostaglandins in the airways of subjects with mild asthma, Am. Rev. Respir. Dis. 142 (1990) 126–132.
[29] A. Szczeklik, S. Kladek, R. Dworski, E. Nizankowska, J. Soja, J. Sheller, J. Oates, Bronchial aspirin challenge causes specific eicosanoid response in aspirin-sensitive asthmatics, Am. J. Respir. Crit. Care Med. 154 (1996) 1608–1614.

Int. J. Radiation Oncology Biol. Phys., Vol. 74, No. 1, pp. 229–236, 2009

0360-3016/09/$–see front matter

ELSEVIER

doi:10.1016/j.ijrobp.2008.09.060

BIOLOGY CONTRIBUTION

INDUCTION OF DNA DOUBLE-STRAND BREAKS AND CELLULAR MIGRATION THROUGH BYSTANDER EFFECTS IN CELLS IRRADIATED WITH THE SLIT-TYPE MICROPLANAR BEAM OF THE SPRING-8 SYNCHROTRON

GENRO KASHINO, PH.D.,* TAKESHI KONDOH, M.D., PH.D.,† NOBUTERU NARIYAMA, PH.D.,‡ KEIJI UMETANI, PH.D.,‡ TAKUJI OHIGASHI, PH.D.,‡ KUNIO SHINOHARA, PH.D.,‡§ AI KURIHARA, M.S.,‖ MANABU FUKUMOTO, M.D., PH.D.,‖ HIROKI TANAKA, PH.D.,* AKIRA MARUHASHI, PH.D.,* MINORU SUZUKI, M.D., PH.D.,* YUKO KINASHI, M.D., PH.D.,* YONG LIU, M.D, PH.D.,* SHIN-ICHIRO MASUNAGA, M.D., PH.D.,* MASAMI WATANABE, PH.D.,* AND KOJI ONO, M.D., PH.D.*

*Research Reactor Institute, Kyoto University, Osaka, Japan; †Department of Neurosurgery, Graduate School of Medicine, Kobe University, Kobe, Japan; ‡Japan Synchrotron Radiation Research Institute, Hyogo, Japan; §Advanced Research Institute for Science and Engineering, Waseda University, Tokyo, Japan; and ‖Department of Pathology, Institute of Development, Aging and Cancer, Tohoku University, Sendai, Japan

Purpose: To determine whether glioma cells irradiated with a microplanar X-ray beam exert bystander effects.
Methods and Materials: Microplanar beam irradiation of glioma cells *in vitro* was done using the SPring-8 synchrotron radiation facility. The amount of DNA double-strand breaks (dsbs) was measured by the fluorescence intensity of phosphorylated H2AX or the number of 53BP1 foci. The dose distribution in a cell population exposed to a single microplanar beam was determined by the amount of phosphorylated H2AX-positive cells. Bystander effects were determined by counting the number of 53BP1 foci in nonirradiated cells treated with conditioned medium from cultures of irradiated cells.
Results: More DNA dsbs were detected in cells adjacent to an area irradiated by the single beam than in cells in distant, nonirradiated areas as a result of bystander effects caused by scattered X-rays and DNA dsbs. In support of this, more 53BP1 foci were observed in nonirradiated, conditioned medium–treated cells than in control cells (*i.e.*, cells not treated with irradiation or conditioned medium). These results suggest that DNA dsbs were induced in nonirradiated cells by soluble factors in the culture medium. In addition, we observed cellular migration into areas irradiated with peak doses, suggesting that irradiated cells send signals that cause nonirradiated cells to migrate toward damaged cells.
Conclusions: Bystander effects are produced by factors secreted as a result of slit-type microplanar X-ray beam irradiation. © 2009 Elsevier Inc.

Bystander effect, Slit microbeam, Radiotherapy, DNA double-strand breaks, Cellular migration.

INTRODUCTION

Theoretically, synchrotron X-ray beams permit the delivery of very high radiation doses to tumors in a single fraction using arrays of microplanar X-ray beams (1, 2). Because the normal tissue effects associated with microplanar beam use appear to be reduced while its tumor cell killing effect is clearly potent, this technology is widely expected to form the basis of a new approach to radiotherapy (3). To realize the full potential of this new radiotherapy technique, it is important to identify the biologic mechanisms responsible for its potent tumor cell killing but minimal normal tissue effect.

Evidence for a bystander effect, in which irradiated cells produce signals that affect nonirradiated cells in the same population, continues to accumulate (4–17), and this promises to hold true for slit-type microplanar beam irradiation as well. Several groups of researchers have reported that factors secreted from irradiated cells appear to mediate the bystander effects in nonirradiated cells (7, 13–16). There are also some evidence that DNA double-strand breaks (dsbs) are induced by these factors (13–16), but neither of these phenomena has been clearly shown.

In the present study, cultured C6 glioma cells were subjected to microplanar irradiation, after which biologic

Reprint requests to: Genro Kashino, Particle Radiation Oncology Research Center, Research Reactor Institute, Kyoto University, 2-1010 Asashiro Nishi, Kumatori-cho, Sennan-gun, Osaka 590-0458, Japan. Tel: +81-72-451-2425; Fax: +81-72-451-2627; E-mail: kashino@rri.kyoto-u.ac.jp

Conflict of interest: none.

Acknowledgments—The authors are grateful to the program of Medical Bio Trial Use by Japan Synchrotron Radiation Research Institute. This work was also supported by KAKENHI 19790870.

Received July 18, 2008, and in revised form Sept 11, 2008. Accepted for publication Sept 30, 2008.

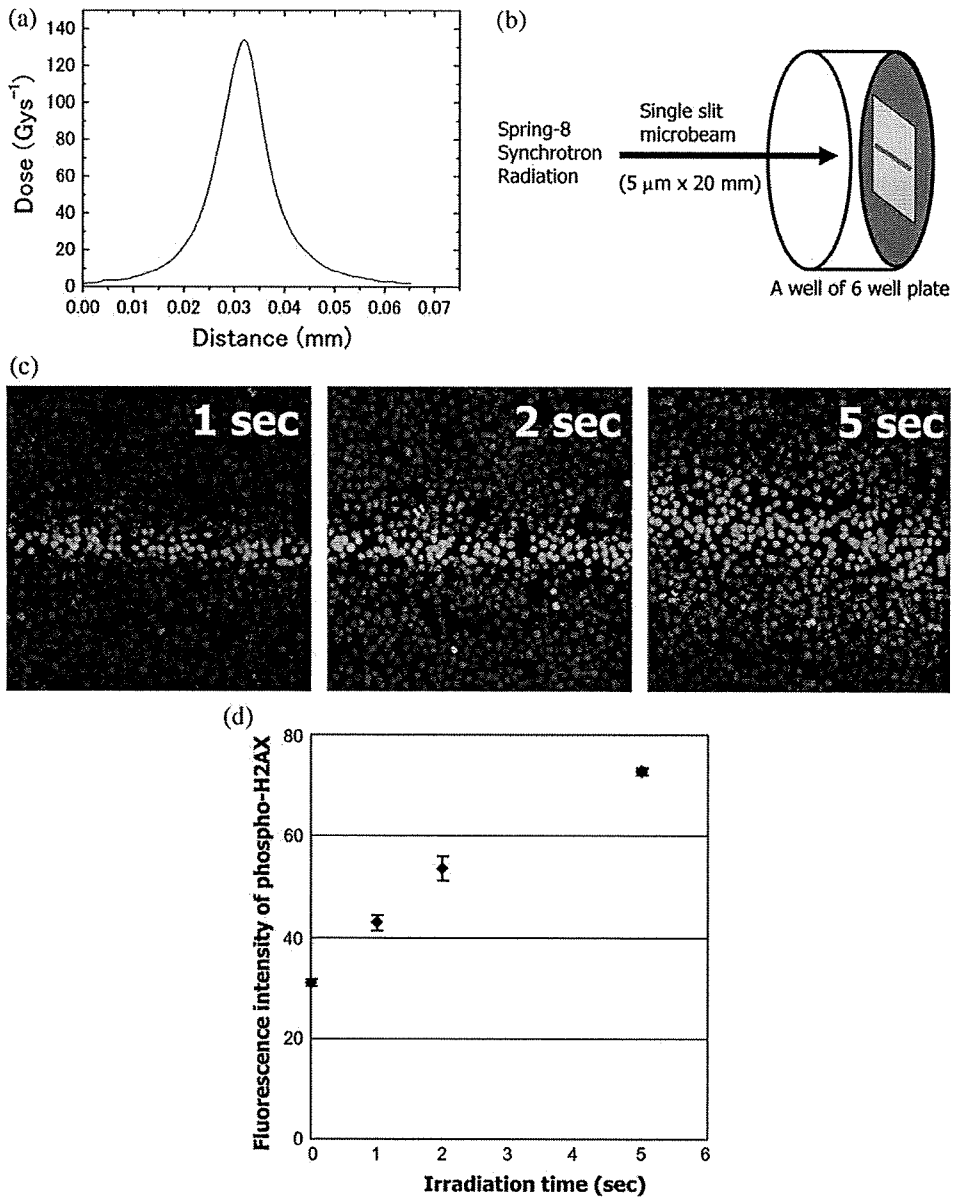

Fig. 1. (a) Dose distribution of single-slit–irradiated cells in the collimated region was determined by X-ray film analysis. (b) Schema of the slit irradiation experiment. The SPring-8 synchrotron radiation beam goes straight through a slit-type collimator and confluent cells on the cover slip were irradiated. (c) Images of cells irradiated with a single-slit microplanar beam for the indicated times. Fluorescence from phospho-H2AX (green) is seen along the beam-irradiated area, in addition to DAPI-stained nuclei (blue). Magnification ×200. (d) Fluorescence intensities of phospho-H2AX for each irradiation period. At a dose rate of 137 Gy/s, 1-, 2-, and 5-s irradiation periods correlated with doses of 137, 374, and 685 Gy in the peak area, respectively.

dosimetry of the irradiated area was performed to distinguish direct radiation effects from bystander responses. Our results showed that factors secreted by glioma cells exposed to microplanar beam irradiation produce DNA dsbs in neighboring cells, thereby elucidating the mechanism of the bystander effects of irradiation that lead to enhanced cell killing.

METHODS AND MATERIALS

Microplanar beam irradiation at SPring-8

The SPring-8 synchrotron facility (BL28B2 line) was used to supply microplanar beam irradiation. The synchrotron radiation beam traveled in a vacuum transport tube to minimize unwanted air scattering of the primary beam; X-rays came out from the vacuum tube into the atmosphere by passing through a beryllium vacuum window, a 2.0-m helium beam path consisting of an aluminum tube and a thin aluminum helium window that was located 42 m from the synchrotron radiation output. This beamline produces nearly parallel X-rays, and the cells were irradiated at a position 2.5 m from the thin aluminum window. White beam X-rays with an energy level of approximately 100 keV were derived through 3-mm Cu absorbance. Cells were irradiated with a single slit collimator or multi-slit collimator. The dose distribution of single slit irradiation is shown in Fig. 1. The dose rate was 137 Gy/s at the peak. The multi-slit collimator, which produces four peak dose areas

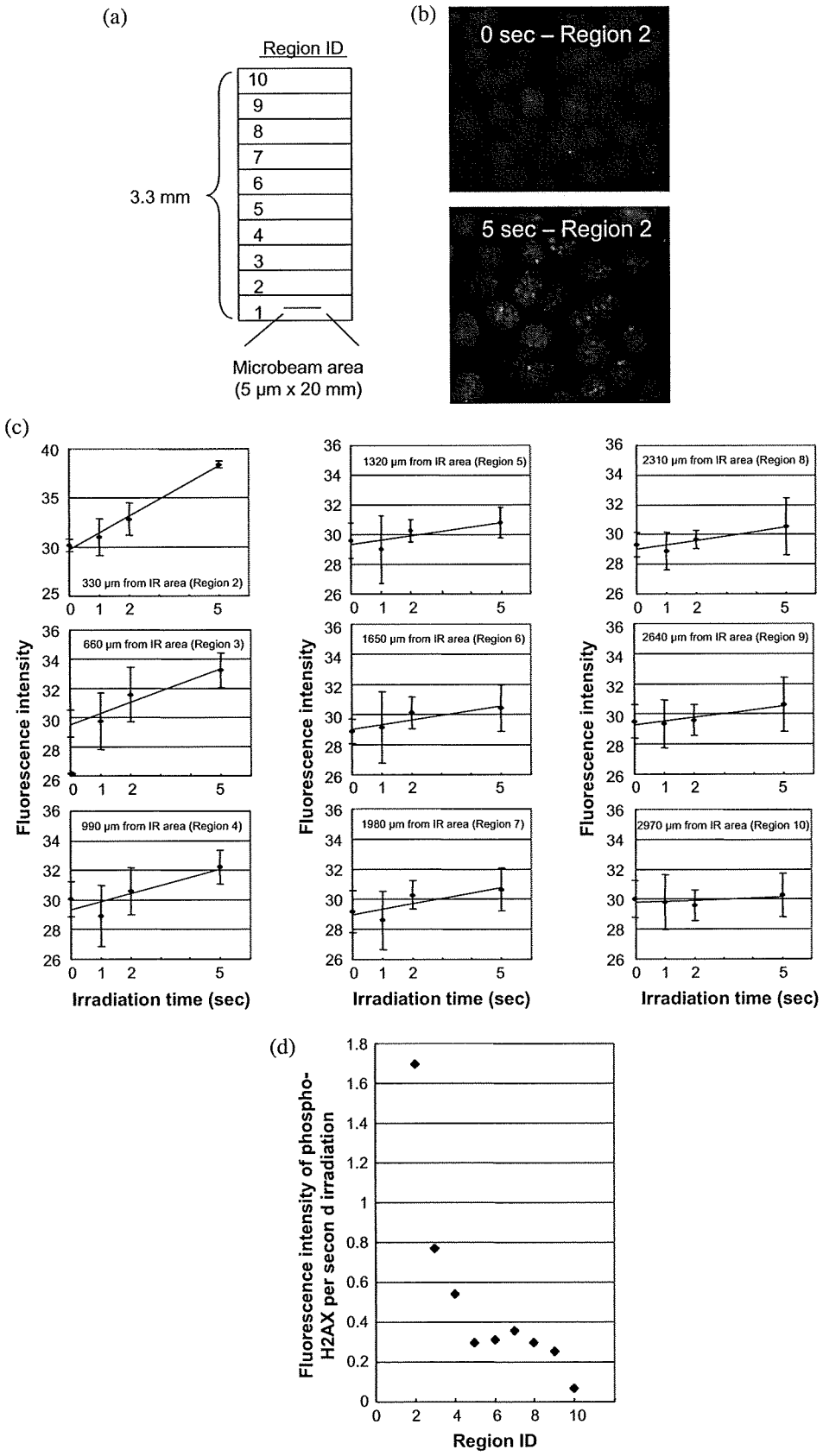

Fig. 2. Bio-dosimetry analysis of the intensity of phospho-H2AX fluorescence around the microbeam-irradiated areas. (a) The area, 3.3 mm in length, was separated into 10 regions, and the average fluorescence intensity for the cell populations in each region was examined. (b) Images of nonirradiated (upper) and 5 s–irradiated (lower) samples from region 2. (c) The

composed of 25 μm width each to process the microplanar beam, was set downstream of the output of the beam line hatch. Kapton (polyimide) films (25 μm) were put in the tungsten collimator at 175-μm intervals. In the case of the multi-slit microplanar beam, the dose rate of X-rays through this collimator was approximately 110 Gy/s at the peak. The details of this multi-slit irradiation system were described by Ohno *et al.* (22) and Nariyama *et al.* (23).

Cell culture conditions

C6 rat glioma cells and U251 human glioma cells were cultured in T25 flasks or six-well plates. For the immunofluorescent staining assays, cells were cultured on 22 × 22-mm cover slips (Matsunami, Osaka, Japan) in each well of a six-well plate. Cells were cultured in alpha-minimal essential medium (MEM) (Invitrogen, Carlsbad, CA) supplemented with 10% fetal bovine serum (FBS; HyClone Laboratories, Logan, UT) or HFDM-1 serum-free medium (Functional Peptide Institute, Yamagata, Japan) (24). Cells were maintained at 37°C in a humidified atmosphere with 5% CO_2.

Detection of DNA dsbs by immunofluorescent staining of phospho-H2AX and 53BP1

For the single-slit irradiation experiment, cells on 22 × 22 mm cover slips in six-well plates were incubated with 2 ml of alpha-MEM with 10% FBS and kept under confluent conditions for several days. Cells were then irradiated with single-slit irradiation, as described above. One hour after irradiation, the cells were fixed with 4% formaldehyde in phosphate-buffered saline (PBS), permeabilized for 10 min on ice in 0.5% Triton X-100 in PBS, and washed extensively with PBS. The cover slips were then incubated with anti-phosphorylated histone H2AX (serine 139) antibody (Upstate Biotechnology, NY) or anti-53BP1 antibody (Bethyl Laboratories, Montgomery, TX) in TBS-DT (20 mmol/l Tris-HCl, 137 mmol/l NaCl, pH 7.6, containing 50 mg/ml skim milk and 0.1% Tween-20) for 2 h at 37°C. The primary antibodies were washed with PBS, and Alexa Fluor 488–labeled anti-mouse IgG and Alexa Fluor 594–labeled anti-rabbit IgG secondary antibodies (Invitrogen) were added (25–27). The fluorescence intensity of phospho-H2AX was determined in the irradiated populations for a 330 × 436-μm area containing a 5 μm × 20 mm collimated beam area. The cover slips were incubated for 1 h at 37°C, washed with PBS, and sealed onto glass slides with 0.05 ml of PBS containing 10% glycerol (Wako, Osaka, Japan) and 2 μg/ml DAPI (4',6-diamidino-2-phenylindole; Invitrogen) (25–27). The cells were examined using OLYMPUS fluorescence microscope, AX80 and KEYENCE BZ-9000 and the green intensity of the phospho-H2AX signal on digitized images was analyzed using Adobe Photoshop, version 7.0. The average intensities of the green phospho-H2AX signals of cell populations in the same image were determined by histogram analysis in Adobe Photoshop. Thirty images from three independent samples were analyzed in each region.

Cell migration analysis

For the cell migration analysis, performed to assess to what extent cell migration plays a role in the bystander effect, cells on 22 × 22–mm cover slips in six-well plates were incubated with 2 ml of alpha-MEM with 10% FBS and kept in the confluent state for a few days. The cells were then washed with PBS and incubated with 2 ml of HFDM-1 serum-free medium for 24 h before multi-slit irradiation. The cells were next incubated with 2 ml of HFDM-1 medium for 2, 4, 24, or 48 h after irradiation, after which they were fixed with 4% formaldehyde in PBS and immunofluorescent staining performed as described above. Damaged cells were determined by the green fluorescence of phospho-H2AX.

Medium transfer experiment

A medium transfer experiment was performed to verify that any observed bystander effect was responsible for the induction of DNA dsbs in cells neighboring irradiated cells. To exclude the effects of serum in culture medium, serum-free culture was applied after the cells grew to confluence. To collect soluble factor(s) in conditioned medium, multi-slit microplanar beam irradiation was used in the medium transfer experiment. These medium transfer experiments were performed basically as described previously (13, 14, 28) and were done to assess to what extent factors in the growth medium of irradiated cells were responsible for the bystander effects. In the present experiment, cells in T25 flasks were incubated with 5 ml of alpha-MEM with 10% FBS and kept under confluent conditions for several days. The cells were then washed with PBS, cultured in 5 ml of HFDM-1 serum-free medium for 24 h, irradiated with a multi-slit collimator, and cultured without a medium change for a further 24 h. In parallel, confluently growing C6 and U251 cells on 22 × 22–mm cover slips in six-well plates were cultured in 2 ml of normal medium, after which these cells were washed with PBS and then treated with 2 ml of the conditioned medium from the multi-slit collimator–irradiated cells in the T25 flasks. These nonirradiated cells were then incubated for 24 h in the conditioned medium, washed with PBS, and fixed with 4% formaldehyde in PBS. Immunofluorescent staining for 53BP1, which is a marker for dsbs, was performed as described above, and the numbers of red foci were counted to determine the 53BP1 signal. Figure 4a shows typical 53BP1 focion DAPI stained nuclei findings.

Statistical analysis

Statistical analysis was performed using Student's *t* test. Significance was set at a value of $p < 0.05$.

RESULTS

Immunofluorescent study results

Irradiated C6 cells were detected as phospho-H2AX–positive foci (18, 19) in a dose-dependent manner (Fig. 1c). Interestingly, however, the width of areas of confluently growing C6 cells showing phospho-H2AX–positive foci was in accordance with the dose, even under single-slit irradiation conditions (Fig. 1c). This means that the 5-μm width of the collimation dose not only covered the 5-μm width of the irradiated area but also extended to cells neighboring the irradiated area. The number of positive cells with higher phospho-H2AX fluorescence intensities increased in a dose-dependent manner between 1 and 5 s of irradiation (Fig 1d).

relationship between irradiation time and phospho-H2AX fluorescence intensity in all regions. The average values of the phospho-H2AX fluorescence intensities were obtained from 30 cell populations for each region in three independent experiments. Indicated distances in each panel represent the distances between the middle of each region and the irradiated position. (d) Graph summarizing the relationship between each region (distance from microbeam area) and fluorescence intensity. The fluorescence intensity for phospho-H2AX per second was obtained from the graph (see Fig. 2c) of the relationship between irradiation time and fluorescence intensity.

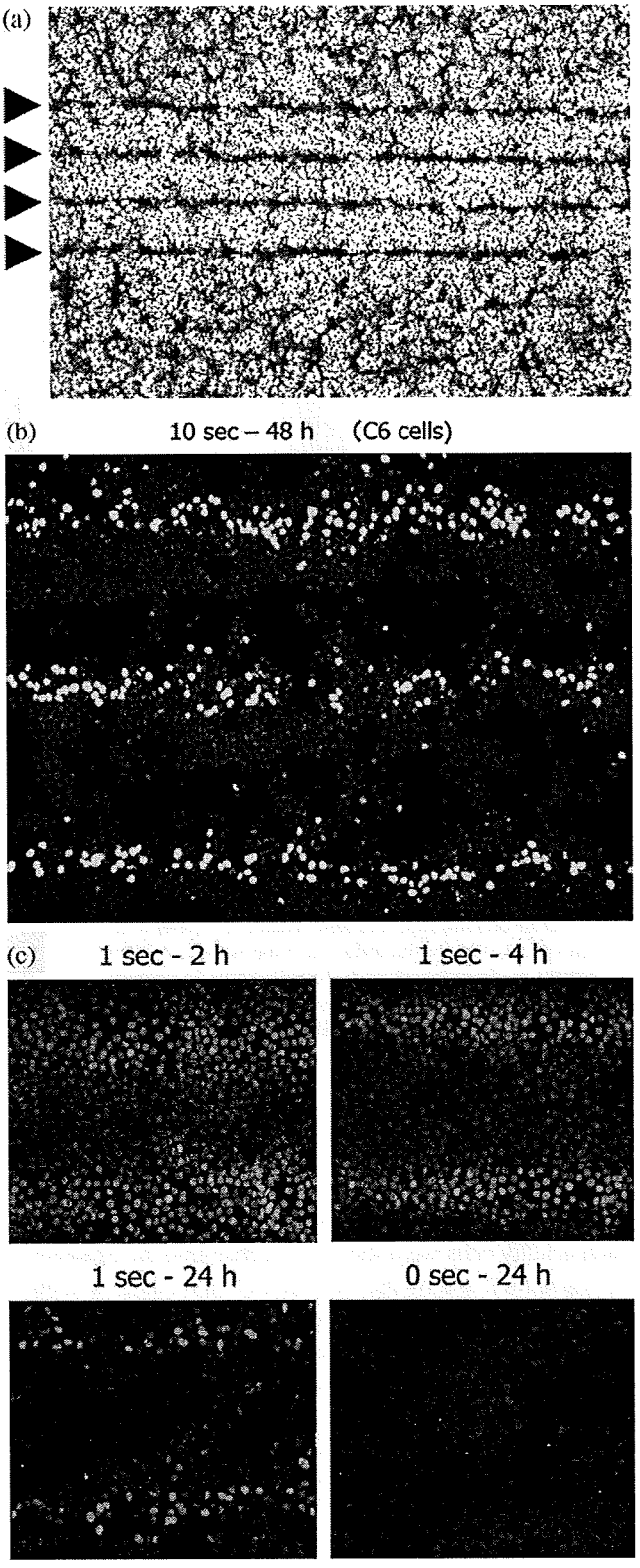

Fig. 3. (a) Images of cellular migration in the populations irradiated with a multi-slit-type microplanar beam. C6 cells were irradiated, fixed for 48 h after 10 s of irradiation, and stained with 3% Giemsa. The positions indicated are the four microbeam-irradiated areas with intervals of approximately 200 μm. (b) Image of phospho-H2AX (green) in DAPI-stained nuclei (blue). C6 cells were irradiated and then fixed 48 h after 10 s of irradiation. (c) Image of phospho-H2AX (green) in DAPI-stained nuclei (blue). Cells (U251) were irradiated and then fixed at 2, 4, and 24 h after 1 s of irradiation.

Relationship of distance from collimated beam and radiation dose

Next, we examined the relationship between the distance from the collimated beam area and the radiation dose. To estimate the irradiation intensity in each area (330 × 436 μm) no more than 3.3 mm from the collimated beam area, the area was separated into 10 regions, and then the fluorescence intensity of phospho-H2AX in each region was examined (Fig. 2a). The results of the fluorescence intensity analysis at 330, 660, 990, 1320, 1650, 1980, 2310, 2640, and 2970 μm from the beam center (Areas 2, 3, 4, 5, 6, 7, 8, 9, and 10, respectively) are summarized in Fig. 2c. These results showed a linear increase in fluorescence that occurred in a dose-dependent manner, suggesting that the cells were exposed to radiation effects even at 2 to 3 mm from the beam center. Figure 2d summarizes these findings and shows that the fluorescence intensities of phospho-H2AX were still higher in irradiated than in nonirradiated cells even in Region 9, which was about 2640 μm from the beam center. In addition, there was no decrease in the fluorescence intensity between Regions 5 and 9, despite a clear observation of a decrease within Regions 1 to 4. This suggests that bystander effects may exist even in regions adjacent to single-slit–irradiated cells.

Cell migration analysis

As shown in Fig. 3a, four condensed bands were observed 48 h after irradiation along the periphery of C6 cells irradiated with the multi-slit microplanar beam. This suggested that the cells surrounding the beam center had migrated closer to the beam center after irradiation. Both irradiated and damaged cells were detected in these lines of cells, indicating fluorescence phospho-H2AX positivity 48 h after 10 s of irradiation and clearly showing that cells had gathered near the damaged cells (Fig. 3b). As shown in Fig. 3c, nondamaged U251 cells migrated toward the phospho-H2AX–positive cells (*i.e.*, damaged cells) at 24 h after irradiation, but this migration was not seen at earlier time points. These results showed that secreted factor(s) were present in the culture medium of cells exposed to multi-slit microplanar beam irradiation and that healthy cells were stimulated by these factor(s) to migrate gradually toward the damaged cells.

dsbs Analysis

As shown in Fig. 4b, 53BP1 foci formation (20, 21) was observed in C6 cells treated with conditioned medium from the culture of cells exposed to multi-slit microplanar beam irradiation, and these effects were dose dependent. These results suggest that factors secreted by cells in response to slit-type microplanar beam irradiation can induce DNA dsbs in nonirradiated cells through a bystander effect.

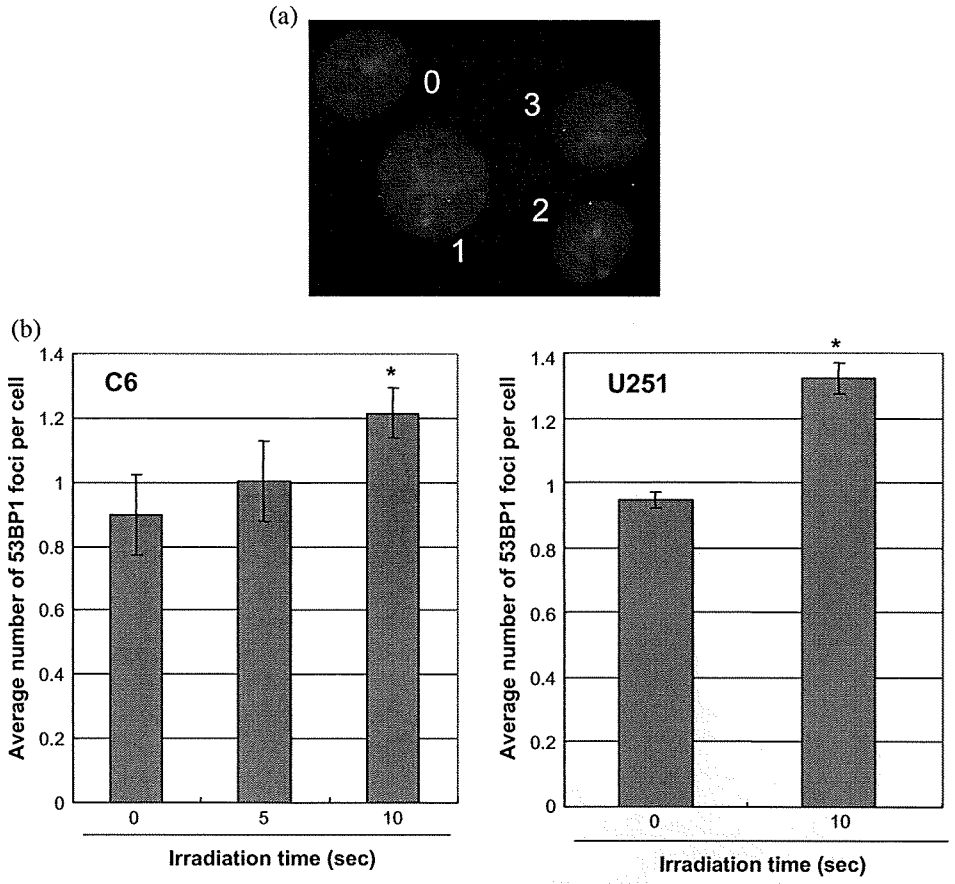

Fig. 4. Results of the medium transfer experiment. (a) Image of 53BP1 foci (red) in DAPI-stained nuclei (blue). The numbers of foci in each nucleus are indicated. (b) The numbers of 53BP1 foci in conditioned-medium–treated C6 (left) and U251 (right) cells. Each conditioned medium was obtained from cultures irradiated for the indicated time period at 24 h after irradiation, and the incubation of nonirradiated cells with conditioned medium lasted 24 h. Results show the mean number ± the standard error of the mean (SEM) of 53BP1 foci from three independent experiments. Significant differences were observed between the number of cells treated with conditioned medium from nonirradiated cells (0 s) and that from irradiated cells (10 s) (*Student's t test, $p < 0.05$).

DISCUSSION

Our findings suggest that cell migration and DNA dsbs formation were both induced by bystander effects in response to slit-type microplanar beam irradiation. This is, to our knowledge, the first report showing that synchrotron-based microplanar beam irradiation can induce bystander effects in glioma cells *in vitro,* which indicates the important potential of this technology.

As evident in Figs. 1 and 2, the width of the area of cells that showed a response to single-slit irradiation was greater than the expected one based on the actual beam width, which we attribute to scattered X-rays. This type of exposure was clearly observed within 2640 μm (Area 4) of the 5-μm-wide slit beam area, as shown in Fig. 2c. However, fluorescence intensities did not decrease to more than 990 to 3,000 μm (Regions 5–9 in Fig. 2d) from the irradiation site, despite the higher-than-background levels (0 s of irradiation) of fluorescence (Fig. 2d). If the phosphorylation of H2AX was induced solely by scattered X-rays in Regions 5 to 9, the fluorescence intensity in these areas should have decreased with increasing distance. The fact that phospho-H2AX fluorescence intensities increased in Regions 5 to 9 suggests that irradiation also produced a biologic effect such as a bystander effect.

This was clearly shown by our cellular migration assay, in which healthy cells were found to migrate into the irradiated cell population, and by the induction of DNA dsbs in nonirradiated cells cultured in irradiated cell culture medium (Figs. 3 and 4). However, as the exposed dose and dose rate were extremely high in the present assay, these findings may be a unique response to a synchrotron-based micro-planar beam. In the other migration assay involving conventional X-irradiation, cells did not migrate under the same culture conditions. Therefore, it is not likely that cells irradiated by scattered X-rays are readily able to migrate. Moreover, cellular migration after multi-slit irradiation was not observed for cells cultured in medium with 10% FBS (data not shown), suggesting that the absence of serum factor(s) is important in this migration. In our serum-free HFDM-1 medium experiment, it was observed that the cell numbers in the population did not change during the 24-h incubation, probably because of insufficient levels of growth factors, and it was confirmed

that the total number of cells around the slit-irradiated area at 24 h after irradiation was not increased. However, areas with decreased cell numbers appeared between the two irradiated areas, which suggests that the dense arrangement of nondamaged cells (*i.e.*, phospho-H2AX–negative cells) around damaged cells (*i.e.*, phospho-H2AX–positive cells) was not caused by dividing healthy cells.

Although it is not clear which soluble factor(s) are involved in the cellular migration observed in the present study, transforming growth factor–β (TGF-β) may be a candidate, as it is well known to be induced by irradiation (29, 30) and has been observed to be involved in bystander effects (31, 32). Epidermal growth factor (EGF) may also be a candidate, as both it and TGF-β can synergistically cause cellular migration in human immortalized HK cells (33). However, as HFDM-1 medium contains EGF but not TGF-β, we conjecture that TGF-β is secreted from irradiation-damaged cells.

Because phospho-H2AX is a well-known DNA double-strand marker (18), the fluorescence intensity of phospho-H2AX was used to determine the relative fluorescence intensities of cell populations composed of approximately 500 to 1,000 cells per region (Fig. 2a). This method was particularly useful for the wider biodosimetry analysis in the present study, as shown in Fig. 1d. However, fluorescence has also been detected at sites where chromatin remodeling was occurring under physiologic conditions (25, 34, 35). From the standpoint of the cell-cycle phase, the S-phase can be detected as phospho-H2AX fluorescence in the whole nucleus (26), which makes this method useful for examining the relative differences in irradiation effects. A drawback of this method, however, is that it is difficult to detect small increases in the frequency of DNA dsbs. Thus, the analysis by phospho-H2AX is useful for detecting the increased level of DNA dsbs in a wider area, but not for the small inductions in the single-cell level.

In our comparison of the numbers of 53BP1foci in nonirradiated cells and cells incubated with conditioned medium from slit microplanar beam–irradiated cells, significantly higher numbers of foci were observed for cells treated with 10 s–irradiated conditioned medium compared with cells treated with control medium. There was, however, a small increase in the number of foci observed for cells exposed to medium from 5-s–irradiated cells (Fig. 4b, C6 cells). These results suggest that bystander factors are secreted in an irradiation dose–dependent manner.

Interestingly, cellular migration was not observed in multi-slit–irradiated normal human fibroblast BJ cells (data not shown). The next step in this research into the effects of microplanar beam irradiation should therefore be to clarify the biologic significance of these bystander effects by focusing on the differences between tumor cells and surrounding normal cells.

REFERENCES

1. Laissue JA, Geiser G, Spanne PO, *et al.* Neuropathology of ablation of rat gliosarcomas and contiguous brain tissues using a microplanar beam of synchrotron-wiggler-generated X rays. *Int J Cancer* 1998;78:360–654.
2. Dilmanian FA, Button TM, Le Duc G, *et al.* Response of rat intracranial 9L gliosarcoma to microbeam radiation therapy. *Neuro Oncol* 2002;4:26–38.
3. Dilmanian FA, Qu Y, Liu S, *et al.* X-ray microbeams: Tumor therapy and central nervous system research. *Nucl Instrum Methods Phys Res* 2005;548:30–37.
4. Nagasawa H, Little JB. Induction of sister chromatid exchanges by extremely low doses of alpha-particles. *Cancer Res* 1992;52: 6394–6396.
5. Azzam EI, de Toledo SM, Gooding T, Little JB. Intercellular communication is involved in the bystander regulation of gene expression in human cells exposed to very low fluences of alpha particles. *Radiat Res* 1998;150:497–504.
6. Shao C, Furusawa Y, Aoki M, Ando K. Role of gap junctional intercellular communication in radiation-induced bystander effects in human fibroblasts. *Radiat Res* 2003;160:318–323.
7. Mothersill C, Seymour C. Medium from irradiated human epithelial cells but not human fibroblasts reduces the clonogenic survival of unirradiated cells. *Int J Radiat Biol* 1997;71: 421–427.
8. Shao C, Furusawa Y, Aoki M, *et al.* Nitric oxide-mediated bystander effect induced by heavy-ions in human salivary gland tumour cells. *Int J Radiat Biol* 2002;78:837–844.
9. Shao C, Stewart V, Folkard M, *et al.* Nitric oxide-mediated signaling in the bystander response of individually targeted glioma cells. *Cancer Res* 2003;63:8437–8442.
10. Shao C, Folkard M, Michael BD, Prise KM. Targeted cytoplasmic irradiation induces bystander responses. *Proc Natl Acad Sci USA* 2004;101:13495–13500.
11. Schettino G, Folkard M, Prise KM, *et al.* Low-dose studies of bystander cell killing with targeted soft X rays. *Radiat Res* 2003;160:505–511.
12. Schettino G, Folkard M, Michael DB, Prise KM. Low-dose binary behavior of bystander cell killng after microbeam irradiation of a single cell with focused c(k) X-rays. *Radiat Res* 2005; 163:332–336.
13. Kashino G, Prise KM, Schettino G, *et al.* Evidence for induction of DNA double strand breaks in the bystander response to targeted soft X-rays in CHO cells. *Mutat Res* 2004;556:209–215.
14. Kashino G, Suzuki K, Matsuda N, *et al.* Radiation induced bystander signals are independent of DNA damage and DNA repair capacity of the irradiated cells. *Mutat Res* 2007;619: 134–138.
15. Ryan LA, Smith RW, Seymour CB, Mothersill CE. Dilution of irradiated cell conditioned medium and the bystander effect. *Radiat Res* 2008;169:188–196.
16. Yang H, Asaad N, Held KD. Medium-mediated intercellular communication is involved in bystander responses of X-ray-irradiated normal human fibroblasts. *Oncogene* 2005;24: 2096–2103.
17. Hamada N, Matsumoto H, Hara T, Kobayashi Y. Intercellular and intracellular signaling pathways mediating ionizing radiation-induced bystander effects. *J Radiat Res* 2007;48:87–95.
18. Rothkamm K, Löbrich M. Evidence for a lack of DNA double-strand break repair in human cells exposed to very low x-ray doses. *Proc Natl Acad Sci U S A* 2003;100:5057–5062.
19. Burdak-Rothkamm S, Short SC, Folkard M, *et al.* ATR-dependent radiation-induced gamma H2AX foci in bystander primary human astrocytes and glioma cells. *Oncogene* 2006;25:7336–7342.
20. Huyen Y, Zgheib O, Ditullio RA Jr., *et al.* Methylated lysine 79 of histone H3 targets 53BP1 to DNA double-strand breaks. *Nature* 2004;432:406–411.

21. Botuyan MV, Lee J, Ward IM, *et al.* Structural basis for the methylation state-specific recognition of histone H4-K20 by 53BP1 and Crb2 in DNA repair. *Cell* 2006;127:1361–1373.
22. Ohno Y, Torikoshi M, Suzuki M, *et al.* Dose distribution of a 125 keV mean energy microplanar x-ray beam for basic studies on microbeam radiotherapy. *Am Med Phys* 2008;35:3252–3258.
23. Nariyama N, Ohigashi T, Umetani K, *et al.* Spectromicroscopic film dosimetry for high-energy microbeam from synchrotronradiation. *Appl Radiat Isot* 2009;67:155–159.
24. Yamada K, Yamaura J, Katoh M, *et al.* Fabrication of cultured oral gingiva by tissue engineering techniques without materials of animal origin. *J Periodontol* 2006;77:672–677.
25. Suzuki M, Suzuki K, Kodama S, Watanabe M. Phosphorylated histone H2AX foci persist on rejoined mitotic chromosomes in normal human diploid cells exposed to ionizing radiation. *Radiat Res* 2006;165:269–276.
26. Suzuki K, Okada H, Yamauchi M, *et al.* Qualitative and quantitative analysis of phosphorylated ATM foci induced by low-dose ionizing radiation. *Radiat Res* 2006;165:499–504.
27. Yamauchi M, Oka Y, Yamamoto M, *et al.* Growth of persistent foci of DNA damage checkpoint factors is essential for amplification of G1 checkpoint signaling. *DNA Repair* 2008;7:405–417.
28. Kashino G, Prise KM, Suzuki K, *et al.* Effective suppression of bystander effects by DMSO treatment of irradiated CHO cells. *J Radiat Res* 2007;48:327–333.
29. Anscher MS, Crocker IR, Jirtle RL. Transforming growth factor-β1 expression in irradiated liver. *Radiat Res* 1990;122: 77–85.
30. Barcellos-Hoff MH. Radiation-induced transforming growth factor β and subsequent extracellular matrix reorganization in murine mammary gland. *Cancer Res* 1993; 53:3880–3886.
31. Iyer R, Lehnert BE, Svensson R. Factors underlying the cell growth-related bystander responses to alpha particles. *Cancer Res* 2000;60:1290–1298.
32. Shao C, Folkard M, Prise KM. Role of TGF-beta1 and nitric oxide in the bystander response of irradiated glioma cells. *Oncogene* 2008;27:434–440.
33. Tian YC, Chen YC, Chang CT, *et al.* Epidermal growth factor and transforming growth factor-beta1 enhance HK-2 cell migration through a synergistic increase of matrix metalloproteinase and sustained activation of ERK signaling pathway. *Exp Cell Res* 2007;313:2367–2377.
34. Ward IM, Chen J. Histone H2AX is phosphorylated in an ATR-dependent manner in response to replicational stress. *J Biol Chem* 2001;276:47759–47762.
35. Stiff T, Walker SA, Cerosaletti K, *et al.* ATR-dependent phosphorylation and activation of ATM in response to UV treatment or replication fork stalling. *EMBO J* 2006; 25:5775–5782.

Journal of Biomechanical Science and Engineering

Vol. 4, No. 1, 2009

Cavitation Bubbles Mediated Molecular Delivery During Sonoporation*

Tetsuya KODAMA**, Yukio TOMITA***, Yukiko WATANABE**, Kenichiro KOSHIYAMA****, Takeru YANO***** and Shigeo FUJIKAWA******

**Graduate School of Biomedical Engineering, Tohoku University, Japan,
2-1 Seiryo, Aoba, Sendai 980-8575, Japan
E-mail: kodama@bme.tohoku.ac.jp
***Faculty of Education, Hokkaido University of Education, Japan,
****Graduate School of Engineering Science, Osaka University, Japan,
*****Graduate School of Engineering, Osaka University, Japan,
******Graduate School of Engineering, Hokkaido University, Japan

Abstract

Molecular delivery using ultrasound (US) and nano/microbubbles (NBs), i.e., sonoporation, has applications in gene therapy and anticancer drug delivery. When NBs are destructed by ultrasound, the surrounding cells are exposed to mechanical impulsive forces generated by collapse of either the NBs or the cavitation bubbles created by the collapse of NBs. In the present study, experimental, theoretical and numerical analyses were performed to investigate cavitation bubbles mediated molecular delivery during sonoporation. Experimental observation using lipid NBs indicated that increasing US pressure increased uptake of fluorescent molecules, calcein (molecular weight: 622), into 293T human, and decreased survival fraction. Confocal microscopy revealed that calcein molecules were uniformly distributed throughout the some treated cells. Next, the cavitation bubble behavior was analyzed theoretically based on a spherical gas bubble dynamics. The impulse of the shock wave (i.e., the pressure integrated over time) generated by the collapse of a cavitation bubble was a dominant factor for exogenous molecules to enter into the cell membrane rather than bubble expansion. Molecular dynamics simulation revealed that the number of exogenous molecules delivered into the cell membrane increased with increasing the shock wave impulse. We concluded that the impulse of the shock wave generated by cavitation bubbles was one of important parameters for causing exogenous molecular uptake into living cells during sonoporation.

Key words: Nanoparticles, Membrane Permeabilization, DDS, Fluorescence

1. Introduction

Nano/microbubbles (NBs) are encapsulated gas bubbles with a radius between 50 nm and 5 μm. These bubbles oscillate nonlinearly in an ultrasound (US) field and emit acoustic signals with harmonic and subharmonic components, on the basis of which their acoustic scattering and vasculature signatures are distinguished [1]. The shell membrane of NBs is composed of albumin, lipid, or polymer. The gas inside the bubble is either air or perfluorocarbons. Large molecules such as C_3F_8 prolong enhancement time because of decreased diffusion [2][3]. Ligands that are able to bind disease-related markers can be incorporated on the surface of the bubbles; thus, the bubbles can have an active function to move toward the target sites [4]. Several engineered bubbles that are aimed at targeting inflammation, angiogenesis, early tumor formation, and thrombi have been reported in the

*Received 22 July, 2008 (No. 08-0493)
[DOI: 10.1299/jbse.4.124]

literature [5].

NBs have been used to modulate targeted molecular mediators. Conceptually, NBs are mixed with exogenous molecules such as therapeutic genes or anticancer drugs and injected either locally or systemically. Targeted gene transfer is then achieved by destructing NBs located in a selective defined area [6][7][8]. The mechanical index (*MI*) for destructing NBs is reported to be 0.1 - 0.5 [9][10][11][12], where *MI* is defined as the peak negative pressure divided by the square root of the US frequency. The efficiency of molecular delivery depends on the US parameters (exposure time, intensity, pulse length, and duty cycle of US) [13][14], the membrane components of the NBs [15][16], and the cell-to-NB ratio [17][18].

Collapse of NBs generates second products such as many tiny bubbles as well as debris that have gas attached or included as modeled by Harvey *et al.*[19]. Since NBs and the second products behave as cavitation nuclei [20][21][22], cavitation bubbles generate from them in a field of US. Broadband noise measurements detected the generation of cavitation bubbles in the presence of US with varying pressures from 0.5 to 2.0 MPa [23].

NBs and cavitation bubbles generate mechanical forces such as bubble expansion, microstreaming, liquid jet impact, and shock waves. These forces interact with the surrounding cells, resulting in transient membrane permeability, followed by the entry of exogenous molecules [24][25][26].

The pressure profile of a shock wave indicates its energy content, and shock-wave propagation in tissue is associated with cellular displacement, leading to the development of cell deformation. The efficiency of molecular delivery depends on the molecular size of exogenous molecules [27][28], and the application time of shock waves [28][29]. Kodama et al. [30] reported that the impulse of the shock wave (i.e., the pressure integrated over time) was a dominant factor for membrane permeability. Molecular dynamics (MD) simulation has shown that shock wave impulse induces water molecule penetration [31][32] and formation of transient water pores in a lipid bilayer [33].

In the present study, experimental, theoretical and numerical analyses were performed to investigate cavitation bubbles mediated molecular delivery during sonoporation. The impulse of the shock wave generated by cavitation bubbles was shown as one of important parameters for causing exogenous molecular uptake into living cells in sonoporation.

2. Materials & Methods

2.1. Experiment

Ultrasound

US was generated at 1.0 MHz by using a 12-mm-diameter submersible piezoceramic transducer (Fuji Ceramics Co., Tokyo, Japan) in a test chamber (300 × 450 × 300 mm, L × W × H) filled with tap water. A 1.0-MHz sine wave (sinusoid) was generated using a multifunction synthesizer (WF1946A; NF Co., Yokohama, Japan) and amplified with a high-speed bipolar amplifier (HSA4101; NF Co.). The pressure values were measured using a PVDF needle hydrophone (PVDF-Z44-1000; Specialty Engineering Associates, Soquel, CA, USA) at a standoff distance of 1 mm from the transducer surface. The signals from the hydrophone were amplified and recorded into a digital oscilloscope (500 MHz, 1 MΩ (16 pF), Wave Surfer 454; LeCroy Co., Chestnut, NY, USA). The peak positive acoustic pressures were 0.2, 0.3, and 0.5 MPa, and each pressure corresponded to the calculated acoustic intensity of 1.3, 3.0, and 8.3 W/cm^2, respectively. The intensity was defined as the average rate of energy flow through a unit area normal to the direction of propagation. *MI* was 0.2, 0.3, and 0.5, respectively. The values of the peak positive pressures were the same as those of the peak negative pressures. The duty ratio was 50%; number of pulses, 2000;

pulse repletion frequency (PRF), 250 Hz; and exposure time, 10 s.

Nano/microbubbles

Lipid NBs were created in an aqueous dispersion of 2 mg/mL 1,2-distearoyl-*sn*-glycero-3-phosphocholine (Avanti Polar Lipids, Alabaster, AL, USA) and 1 mg/mL polyethylene glycol 40 stearate (Sigma-Aldrich Co., St. Louis, MO, USA) by using a 20-kHz sonicator (Vibra Cell™; Sonics & Materials, Inc., Danbury, CT, USA) in the presence of C_3F_8 gas. The presence of lipid molecules in the lipid NB surface was confirmed by staining with 3 μM FM1-43 (excitation: 553 nm, emission: 570 nm; Molecular Probe Inc., Eugene, OR, USA) and observation under an inverted microscope (IX81; Olympus Co., Tokyo, Japan). The mean concentration was 3.4×10^8 bubbles/mL. The peak diameters expressed in terms of size distribution and zeta potential were 1272 ± 163 nm (n = 7, mean ± S.D.) and –4.11 ± 0.74 mV (n = 4, mean ± S.D.), respectively (Fig. 1). Both values were measured by using a laser diffraction particle size analyzer (particle range of 0.6 nm –7 μm, ELSZ-2; Otsuka Electronics Co. Ltd, Osaka, Japan) in phosphate-buffered saline without Mg^{2+} and Ca^{2+} (PBS, pH 7.2 at room temperature, Sigma-Aldrich) [34].

Cell culture

In vitro studies were performed in accordance with the ethical guidelines of Tohoku University. Human embryonic kidney (293T) cells were obtained from Prof. M. Ono (Tohoku University, Japan) and were cultured in Dulbecco's modified Eagle's medium (DMEM) containing 10% fetal bovine serum and 1% penicillin-streptomycin in 250 mL culture flasks in a cell culture incubator (SCI-325D; Astec Co., Fukuoka, Japan) at 37°C under an atmosphere of 5% CO_2 in air. Prior to the US-mediated delivery experiments, the total cell counts and viability were determined using a hemocytometer with the trypan blue dye exclusion method [35]. Only cells that were in the exponential growth phase and had a viability of ≥ 99% were used.

Fluorophores

Calcein (622 Da) (excitation: 496 nm, emission: 514 nm; Sigma-Aldrich Co.) was used for the evaluation of the uptake of molecules by the cells in the presence of US and NBs. Calcein was dissolved in PBS and used at a concentration of 200 μM in a complete medium. Stokes radius for calcein was estimated to be 0.68 nm [30].

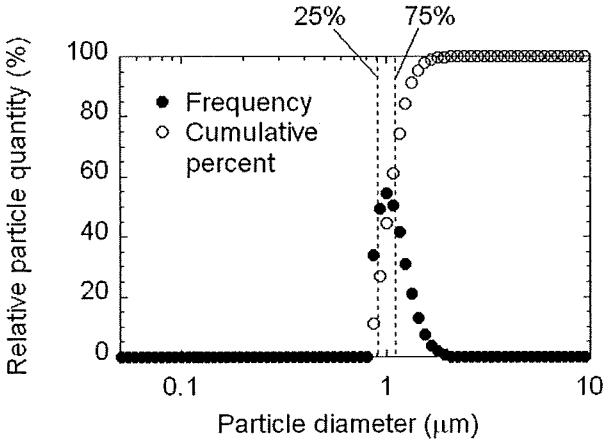

Fig. 1 Size distribution of lipid NBs. The mean peak of size distribution was 1.27 ± 0.431 μm (n = 7, mean ± S. D.). ○: cumulative percent, ●: frequency, n: number of samples.

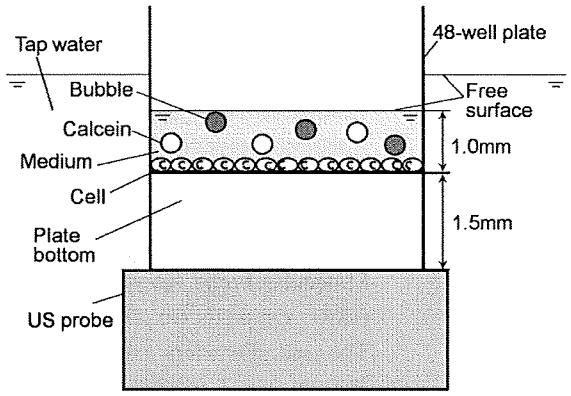

Fig. 2 Experimental setup. The 48-well culture plates were positioned just above the 1-MHz US probe in a test chamber (300 × 450 × 300 mm, L × W × H) filled with water. The basal plate thickness of the 48-well culture plate was 1.5 mm. By assuming the speed of sound in water to be 1500 m/s, we calculated the wavelength as 1.5 mm. The height of the medium containing calcein and lipid NBs in the plate was 1 mm. Complexed superimposed ultrasonic waves were generated in the medium. Atomized particles were generated with increasing US intensity, indicating the generation of cavitation bubbles.

Ultrasound exposure

Cells were seeded onto 48-well plates alternately at 5×10^4 cells/well in a complete medium and incubated at 37°C in a 5% CO_2 incubator. After a 24-h attachment period, the seeded cells were washed with PBS, and the medium was replaced with a fresh medium (110 μL) containing calcein (200 μM) with and without NBs (10% v/v). The height of the medium containing calcein and lipid-micelle bubbles in the plate was 1 mm. The maximum geometrical characteristic radius r_0 occupied uniformly by a single NB (eqn (A2)) for a lipid bubble was calculated to be 19 μm. The US transducer was placed in the test chamber filled with tap water, and the plates were positioned just above the US probe (Fig. 2). The basal plate thickness of the 48-well culture plate was 1.5 mm. When the speed of sound in water was assumed to be 1500 m/s, the wavelength was calculated to be 1.5 mm. Superimposed ultrasonic waves were generated in the media, and atomized particles were generated with increasing US intensity. The generation of particles indicated the generation of cavitation bubbles, as mentioned in the Results and Discussion section. The cells were exposed to US with a pressure of 0.2, 0.3, and 0.5 MPa at a duty ratio of 50% for 10 s. The number of cycles in the pulse was 2000. Twenty-four wells of the 48-well plate were used for each condition. Since the cells were seeded onto alternate wells, the neighboring wells were not exposed to US at the same time. Cell viability was determined using the MTT (3-[4,5-dimethylthiazol-2-yl]-2,5-diphenyltetrazolium bromide) assay as described previously [36], and the cell survival fractions were expressed relative to cells not treated with NBs and US (control).

Fluorescence measurement

After the US exposure, supernatants from 6 wells of the 48-well plate were collected in a 15-mL centrifuge tube. The cells in the wells were washed with 500 μL PBS, and the PBS containing the cells was transferred to the abovementioned centrifuge tubes. All the cells were trypsinized (100 μL/well) and transferred to each centrifuge tube. The cells were washed with PBS (14 mL, 3×) to remove the excess extracellular fluorophore by centrifugation (5 min at 350 × *g*). Then, 1 mL PBS was added to the centrifuge tubes, and the cells were transferred to an eppendorf tube and centrifuged at 8000 × *g* for 5 min. After the supernatant was discarded, the pellet was lyzed with 200 μL of reporter lysis buffer

(Promega, Madison, WI, USA) and subsequently frozen at –80°C for 15 min. The cells were defrosted on ice. Each lysate was centrifuged at 12000 × g for 2 min to pellet cell debris. Twenty microliters of the lysate was analyzed for the uptake of fluorescent molecules by using an Mx3000P™ (Stratagene, La Jolla, CA, USA). The fluorescence was excited using a quartz tungsten halogen lamp (350–750 nm), and the emission was collected through a band-pass filter of 492–516 nm. The fluorescence data was analyzed with MxPro™ QPCR Software (Stratagene). The total protein content in an aliquot of each sample supernatant was calculated with albumin standard curves (BCA protein assay kit; Pierce, Rockford, IL, USA). Two additional standard curves were utilized; one for the cell number and its total protein content, and the other for fluorescence concentration and its fluorescence intensity. Duplicates of the samples and standards were used for the experiment, and the absorption of the protein was measured at 562 nm by using a plate reader (Sunrise; Tecan Austria GmbH, Salzburg, Austria) with the data analysis software LS-PLATEmanager RD (Windows) 2001 (Sunrise). The number of equivalent fluorescent molecules per cell was determined from the calibration curves.

Confocal fluorescence microscopy

293T cells (5 × 10^4 cells/well) were seeded in a complete medium in alternate 48 wells to prevent the exposure of neighboring cells to US. The medium was replaced on the next day with a fresh medium (110 μL) containing calcein (200 μM) with and without NBs (10% v/v). After an US exposure of 10 s, the plates were incubated for 24 h. The cells were then washed 3 times with PBS and trypsinized. Finally, the cell pellet was resuspended in 60 μL of 0.7 μg/mL propidium iodide (PI, excitation: 535 nm, emission: 617 nm, Molecular Probes) and incubated at room temperature for 10-15 min. Confocal fluorescence microscopy was performed using a confocal microscope (FV1000, Olympus). A 60× oil-immersion objective lens with a numerical aperture of 1.25 was used. Calcein and PI fluorescence was excited with a 488-nm line of an argon laser. The laser excitation beam was directed to the specimen through a 488-nm dichroic beam splitter. Emitted fluorescence was collected through a 510- to 550-nm band-pass emission filter for the green channel and a 580-nm long-pass filter for the red channel. Computer-generated images of 1-μm optical sections were obtained at the approximate geometric center of the cell as determined by repeated optical sectioning.

Statistical analysis

All the measurement values are expressed as either mean ± S.D. (standard deviation) or mean ± S.E.M. (standard error of means). Statistical analysis for the calcein uptake was performed by Kruskal-Wallis test. When the Kruskal-Wallis test was significant, the differences between each group were estimated using the Scheff's F test as a post-hoc procedure. The differences were considered to be significant at $P < 0.01$. For the survival fraction, Bartlett test was performed followed by one-way analysis of variance (ANOVA). When the one-way ANOVA was significant, the differences between each group were estimated using the Tukey-Kramer test as a post-hoc procedure. The differences were considered to be significant at $P < 0.05$ or $P < 0.01$.

2.2. Theory

Exposure of cells to US in the presence of NBs generates atomized particles on the surface, indicating the generation of cavitation bubbles [26]. In the medium, NBs and cavitation bubbles interact with each other, and the resulting complex physical forces such as shear stress, liquid jet impact, and shock waves may affect the cell membrane[23][26][37][38][39]. A further investigation of individual physical parameters would lead us into that specialized area of non-spherical bubble dynamics near cell surfaces and